mathematics

MDPI

Article

Buckling Response of Functionally Graded Porous Plates Due to a Quasi-3D Refined Theory

Ashraf M. Zenkour [1,2,*] and Maryam H. Aljadani [1,3]

[1] Department of Mathematics, Faculty of Science, King Abdulaziz University, Jeddah 21589, Saudi Arabia
[2] Department of Mathematics, Faculty of Science, Kafrelsheikh University, Kafrelsheikh 33516, Egypt
[3] Department of Mathematics, Jamoum University Collage, Umm Al-Qura University, Makkah 21421, Saudi Arabia; mhjadani@uqu.edu.sa
* Correspondence: zenkour@kau.edu.sa or zenkour@sci.kfs.edu.eg

Abstract: A quasi-3D refined theory is used to investigate the buckling response of functionally graded (FG) porous plates. The present theory takes into consideration the effect of thickness stretching. Three models of FG porous plates are presented: an isotropic FG porous plate, FG skins with a homogenous core, and an FG core with homogenous skins. The FG porous material properties vary along with the thickness of the FG layer based on modified polynomial law. By using the principle of total potential energy, the equilibrium equations are obtained. The buckling response is determined for simply supported FG porous plates. Analytical investigations are verified to present the accuracy of the current quasi-3D refined theory in predicting the buckling response of FG porous plates. The effect of thickness stretching and several parameters such as porosity coefficients, mechanical loadings, geometric parameters, gradient indexes, and layer thickness ratios are discussed. It is observed that the current theory shows more accurate results for the buckling response of FG plates compared with other shear deformation theories.

Keywords: FG; porous plates; quasi-3D refined theory; buckling

check for updates

Citation: Zenkour, A.M.; Aljadani, M.H. Buckling Response of Functionally Graded Porous Plates Due to a Quasi-3D Refined Theory. *Mathematics* **2022**, *10*, 565. https://doi.org/10.3390/math10040565

Academic Editors: Ioannis Dassios, Clemente Cesarano and Whye-Teong Ang

Received: 10 January 2022
Accepted: 10 February 2022
Published: 11 February 2022

Publisher's Note: MDPI stays neutral with regard to jurisdictional claims in published maps and institutional affiliations.

Copyright: © 2022 by the authors. Licensee MDPI, Basel, Switzerland. This article is an open access article distributed under the terms and conditions of the Creative Commons Attribution (CC BY) license (https://creativecommons.org/licenses/by/4.0/).

1. Introduction

Functionally graded materials (FGMs) are microstructure characteristic materials that involve a spatial variance in the internal structure tailored for a desirable performance or function. A compositionally graded technique gives FGMs superior wear resistance and relatively low density, avoids stress singularities, and interfaces cracking between dissimilar materials. FGMs have received wide applications in biomedical, aerospace, structural, optical, chemistry, and electronic gadgets. An isotropic FG plate has drawn special interest among researchers. A simple refined theory was applied to examine the buckling of FG plates by Daouadji and Adim [1]. Shariat and Eslami [2] reported the FG plates' mechanical and thermal buckling according to the third-order shear deformation theory. Based on refined plate theory and isogeometric analysis, Liu et al. [3] studied FG plate bending and buckling behavior. Bellifa et al. [4] applied a refined four unknowns theory to obtain the buckling behavior of FG plates. Parida and Mohanty [5] investigated FG plate buckling and free vibration response with a Winkler–Pasternak elastic base. Zenkour and Aljadani [6] reported the buckling of FG plates by considering the thickness stretching effect. Sharifan and Jabbari [7] examined the buckling analysis of an FG porous elliptical plate resting on an elastic base.

Sandwich structures with designed face sheets address at least three-layered forms, with a center layer combined with top and bottom designed face sheets. The sandwich structural form is widely used in the automotive, marine engineering, spacecraft, and transportation industries. The vast, growing demands of various sectors for the utilization of low weight-to-strength ratio structures motivated researchers to investigate FG structures with the potential of fulfilling the needs of low-weight and high-strength structures [8].

Therefore, various studies have been conducted to analyze the buckling response of FG sandwich structures. Zenkour [9] used a sinusoidal shear deformation plate theory to report the buckling and free vibration of the FG sandwich plate. Using the meshless method, Neves et al. [10] analyzed the bending, free vibration, and buckling of FG isotropic and sandwich plates. According to the first-order shear deformation theory (FDT), an improved transverse shear stiffness is used to calculate the buckling and vibration responses of FG sandwich plates by Nguyen et al. [11]. Mantari and Monge [12] performed the bending, free vibration, and linear buckling responses of FG sandwich plates. Sobhy [11] presented the vibration and buckling of exponentially graded (EG) sandwich plates laying on an elastic base based on an exponential law distribution and various boundary conditions. Nguyen et al. [13] reported the buckling, bending, and vibration of FG sandwich plates through a refined four-unknown theory and the finite element method. Neves et al. [14] obtained the buckling of FG sandwich plates by considering the thickness stretching effect. Akavci [15] researched the buckling, bending, and vibration of FG sandwich plates according to hyperbolic shear and normal deformations theory. According to three-unknown, non-polynomial shear deformation theory, Bouazza and Zenkour [16] discussed the hygro-thermo-mechanical buckling of a laminated beam using hyperbolic refined shear deformation theory. Nguyen et al. [17] examined the buckling, bending, and free vibration responses of isotropic and FG sandwich plates based on an inverse trigonometric shear deformation theory.

The FG structures can be affected by micro-voids or porosity during the process of manufacturing FG as a result of technical issues. For instance, the pores can be scattered in the internal FG structures during the non-pressure sintering technique [18]. Porous gradient materials have a multifunctional nature, with features such as a high performance-to-weight ratio and shock resistance. However, it is crucial to remember that porosity creates a local loss of stiffness. The most recent progress in manufacturing techniques allows for the fabrication of porous materials with an FG utilizing technologies such as additive 3D printing. As a result, porous materials with specified variable stiffness may be created and adapted for specific technical applications, maximizing performance and decreasing weight [19,20]. Therefore, it is crucial to consider the effect of porosity on the buckling response of FG porous structures, taking into account the presence of porosities in the internal FG structures.

The studies mentioned above considered the perfect FG structures without the presence of porosity inside the structure. However, investigating equipped porous forms of FG sandwich and isotropic structures has been an essential subject of study for researchers. Furthermore, the significant role of these structures in numerous elements of production, such as cost, stability, and reliability, has brought them to the forefront of researchers' attention more than ever before. A few investigations are focused on the buckling of FG porous plates. Kumar et al. [21] used hyperbolic higher-order shear deformation theory to study the buckling and free vibration of FG porous plates resting on an elastic base. In this study, the symmetric center, top, and bottom enhanced porosity distributions were considered. Dhuria et al. [22] studied the static and buckling responses of an FG porous plate subjected to a transverse load. Fan [23] examined the nonlinear buckling and post-buckling load of porous micro- and nano-FG plates. Babaei et al. [24] analyzed the stability analysis of saturated porous FG shells. Tran et al. [25] investigated the bending, buckling, and free vibration responses of FG porous nanoshells resting on an elastic foundation in the context of extended four-unknown, higher-order nonlocal theory. Thom et al. [26] presented the buckling response of cracked FG plates resting on an elastic foundation. Daikh and Zenkour [27] proposed four porosity distributions to report the buckling and free vibration behaviors of FG sandwich plates based on sigmoid and polynomial functions. Chen et al. [28] presented the buckling and bending analysis of FG sandwich plates by employing the Chebyshev–Ritz method and first-order shear deformation plate theory. Xu et al. [29] reported the buckling response of the FG porous core with laminated skins resting on an elastic base. Singh and Harsha [30] used a modified sigmoid model to examine

the buckling of FG sandwich porous plates for three different types of porosity distributions. Mojahedin et al. [31] investigated the buckling response of radially loaded clamped FG circular porous plates. Yang [32] studied the buckling and free vibration response of porous nanocomposite FG plates reinforced with graphene platelets.

As quasi-3D theory includes both shear and normal deformations, various quasi-3D theories have been proposed in the literature. Some studies regarding the different responses of FG structures are reported in [33–43]. However, to the best of the author's knowledge, no prior studies have examined the buckling of FG porous plates with the consideration of the influence of the thickness stretching on the structure, which is essential for thick plate investigation. Therefore, this paper will propose a quasi-3D refined theory to investigate the buckling of isotropic and sandwich FG porous plates. The novelty of this research is to examine the buckling response of various FG plate configurations with porosity using a quasi-3D refined plate theory. The thickness stretching effect is considered in the quasi-3D refined plate theory. Three configurations of FG models are considered: isotropic FG plates, two FG sandwich plates (one is FG faces with a homogenous core), and homogenous faces with an FG core. The present FG porous material properties vary smoothly in the plate thickness direction based on modified polynomial law. The equilibrium equations are obtained according to the principle of total potential energy. The uniaxial and biaxial buckling loadings are reported for simply supported FG plates. The influences of the thickness stretching effect, various porosity parameters, volume fraction exponents, skin-core-skin, and geometric parameters on the critical buckling loads of FG porous plates are reported.

2. Problem Definition and Modeling

2.1. Structural Definition

An FG porous plate of thickness h and cross-sectional $a \times b$ was considered as presented in Figure 1. A Cartesian coordinate system (x, y, z) was adopted to define the plate displacement fields as $0 \le x \le a$, $0 \le y \le b$, and $-h/2 \le z \le h/2$. The FG porous layer was composed of ceramic at the upper plane, and it was continuously varying to metal at the lower plane. The present porous model describes the variation of the materials based on modified polynomial law.

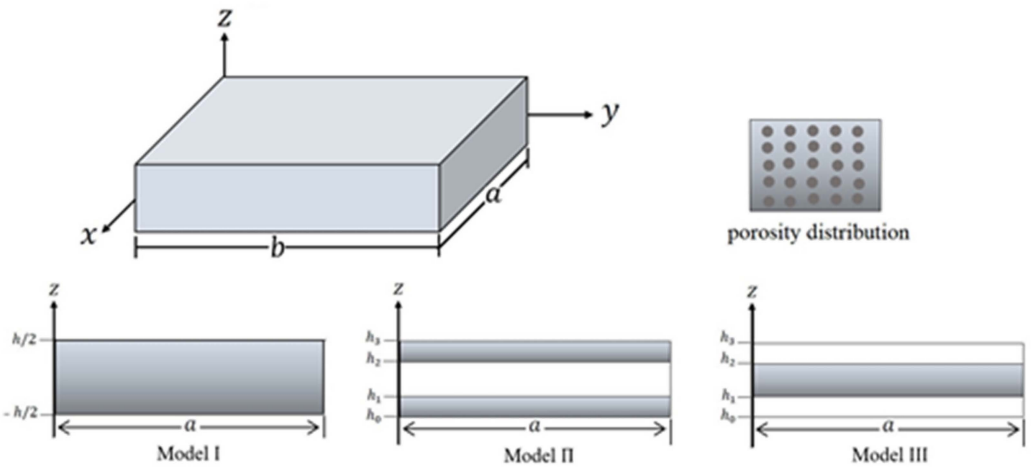

Figure 1. The configurations and geometry of the FG porous plate.

Assuming the porosity is dispersed evenly along the FG structure, the effective material properties of the porous plate based on modified polynomial material law are defined as

$$\mathcal{P} = \mathcal{P}_m\left[V_m(z) - \frac{\xi}{2}\right] + \mathcal{P}_c\left[V_c(z) - \frac{\xi}{2}\right],\ 0 \le \xi \le 1, \tag{1}$$

where $\mathcal{P}$ is the material properties of the porous structure and ξ is a porosity coefficient that describes the pore volume's fraction to the total volume of the structure. In addition, subscripts m and c indicate the constituents of metal as the lower plane and ceramic as the upper plane of the FG layer, respectively. In this paper, three models of FG porous plates are considered:

- Model I: Isotropic FG Plates

This porous model is composed of ceramic at the upper plane ($z = h/2$), and it is continuously varying to metal at the lower plane ($z = -h/2$). The volume fraction of the ceramic is given as

$$V_c = \left(\frac{1}{2} + \frac{z}{h}\right)^k, \; z \in \left[-\frac{h}{2}, \frac{h}{2}\right], \tag{2}$$

where k is the volume fraction exponent and $k \geq 0$.

- Model II: FG Sandwich Plates (FG Faces with a Homogenous Core Plate)

This porous model is composed of FG porous layers at the upper and lower surfaces, while the core is a perfect ceramic. $h_0 = -h/2$ and $h_3 = h/2$ are the lower and upper faces. The volume fraction of the ceramic is given as

$$\begin{gathered} V_c = \left(\frac{z-h_3}{h_2-h_3}\right)^k, \; z \in [h_2, h_3], \\ V_c = 1, \; z \in [h_1, h_2], \\ V_c = \left(\frac{z-h_0}{h_1-h_0}\right)^k, \; z \in [h_0, h_1]. \end{gathered} \tag{3}$$

- Model III: FG Sandwich Plates (Homogenous Faces with an FG Core Plate)

This porous plate is composed of perfect homogenous layers at the upper and lower surfaces, while the core is FG with porosity. $h_0 = -h/2$ and $h_3 = h/2$ are the lower and upper faces. The volume fraction of the ceramic is given as

$$\begin{gathered} V_c = 0, \; z \in [h_2, h_3], \\ V_c = \left(\frac{z-h_1}{h_2-h_1}\right)^k, \; z \in [h_1, h_2], \\ V_c = 1, \; z \in [h_0, h_1]. \end{gathered} \tag{4}$$

2.2. The Quasi-3D Refined Theory

The displacement field of quasi-3D refined theory, taking into account the thickness stretching effect, is expressed as [9]

$$\begin{gathered} u_1(x,y,z) = u(x,y) - z\,\frac{\partial w}{\partial x} + \varphi(z)\theta_x(x,y), \\ u_2(x,y,z) = v(x,y) - z\,\frac{\partial w}{\partial y} + \varphi(z)\theta_y(x,y), \\ u_3(x,y,z) = w(x,y) + \varphi'(z)\theta_z(x,y), \end{gathered} \tag{5}$$

where (u_1, u_2, u_3) represents the displacement field along with the system (x, y, z) in the plate structure, respectively, (u, v, w) represents the displacement projections on the mid-plane along (x, y, z), respectively, and θ_x, θ_y, and θ_z are rotations of the normal to mid-plane about the y-, x-, and z-axes, respectively. The superscript notation $(')$ denotes differentiation concerning z. The present formulation does not require a shear correction factor. Unlike other shear deformation theories, this quasi-3D theory takes under consideration the effect of thickness stretching along with the plate thickness ($\varepsilon_z \neq 0$). The following shape function is considered:

$$\varphi(z) = \frac{\frac{h}{\pi}\sinh\left(\pi\frac{z}{h}\right) - z\cosh\left(\frac{\pi}{2}\right)}{1 - \cosh\left(\frac{\pi}{2}\right)}, \tag{6}$$

The strain relations associated with Equation (6) are given as

$$\begin{gathered}\left\{\begin{array}{c}\varepsilon_x\\ \varepsilon_y\\ \gamma_{xy}\end{array}\right\}=\left\{\begin{array}{c}\varepsilon_x^0\\ \varepsilon_y^0\\ \gamma_{xy}^0\end{array}\right\}+z\left\{\begin{array}{c}\varepsilon_x^1\\ \varepsilon_y^1\\ \gamma_{xy}^1\end{array}\right\}+\varphi(z)\left\{\begin{array}{c}\varepsilon_x^2\\ \varepsilon_y^2\\ \gamma_{xy}^2\end{array}\right\},\\ \left\{\begin{array}{c}\gamma_{yz}\\ \gamma_{xz}\end{array}\right\}=\varphi'(z)\left\{\begin{array}{c}\gamma_{yz}^0\\ \gamma_{xz}^0\end{array}\right\},\ \varepsilon_z\ =\ \varphi''(z)\theta_z\end{gathered} \tag{7}$$

where the components of the strains are in the following forms:

$$\begin{gathered}\left\{\begin{array}{c}\varepsilon_x^0\\ \varepsilon_y^0\\ \gamma_{xy}^0\end{array}\right\}=\left\{\begin{array}{c}\frac{\partial u}{\partial x}\\ \frac{\partial v}{\partial y}\\ \frac{\partial u}{\partial y}+\frac{\partial v}{\partial x}\end{array}\right\},\left\{\begin{array}{c}\varepsilon_x^1\\ \varepsilon_y^1\\ \gamma_{xy}^1\end{array}\right\}=-\left\{\begin{array}{c}\frac{\partial^2 w}{\partial x^2}\\ \frac{\partial^2 w}{\partial y^2}\\ 2\frac{\partial^2 w}{\partial x\partial y}\end{array}\right\},\\ \left\{\begin{array}{c}\varepsilon_x^2\\ \varepsilon_y^2\\ \gamma_{xy}^2\end{array}\right\}=\left\{\begin{array}{c}\frac{\partial\theta_x}{\partial x}\\ \frac{\partial\theta_y}{\partial y}\\ \frac{\partial\theta_x}{\partial y}+\frac{\partial\theta_y}{\partial x}\end{array}\right\},\left\{\begin{array}{c}\gamma_{yz}^0\\ \gamma_{xz}^0\end{array}\right\}=\left\{\begin{array}{c}\theta_y+\frac{\partial\theta_z}{\partial y}\\ \theta_x+\frac{\partial\theta_z}{\partial x}\end{array}\right\}.\end{gathered} \tag{8}$$

The stress–strain constitutive equations of the porous plate when $(\varepsilon_z \neq 0)$ can be written as

$$\left\{\begin{array}{c}\sigma_x\\ \sigma_y\\ \sigma_z\\ \tau_{yz}\\ \tau_{xz}\\ \tau_{xy}\end{array}\right\}^{(r)}=\left[\begin{array}{cccccc}C_{11}&C_{12}&C_{13}&0&0&0\\ C_{12}&C_{22}&C_{23}&0&0&0\\ C_{13}&C_{23}&C_{33}&0&0&0\\ 0&0&0&C_{44}&0&0\\ 0&0&0&0&C_{55}&0\\ 0&0&0&0&0&C_{66}\end{array}\right]^{(r)}\left\{\begin{array}{c}\varepsilon_x\\ \varepsilon_y\\ \varepsilon_z\\ \gamma_{yz}\\ \gamma_{xz}\\ \gamma_{xy}\end{array}\right\} \tag{9}$$

where $(\sigma_i,\ \tau_{ij})$ represents the in-plane normal and shear stresses, $(\gamma_{ij},\varepsilon_i)$ represents the in-plane normal and shear strains of the plate, and $(i,\ j = x,\ y$ and $z)$, $(r = 1,2,3)$ in the case of a sandwich structure. The three-dimensional elastic constants are written as

$$\begin{gathered}c_{11}^{(r)}=c_{22}^{(r)}=c_{33}^{(r)}=\frac{\left(1-\nu^{(r)}(z)\right)E^{(r)}(z)}{\left(1+\nu^{(r)}(z)\right)\left(1-2\nu^{(r)}(z)\right)},\\ c_{12}^{(r)}=c_{13}^{(r)}=c_{23}^{(r)}=\nu c_{11}^{(r)},c_{44}^{(r)}=c_{55}^{(r)}=c_{66}^{(r)}=\frac{E^{(r)}(z)}{2\left(1+\nu^{(r)}(z)\right)}.\end{gathered} \tag{10}$$

If the stretching effect is ignored $(\varepsilon_z \neq 0)$, the elastic constants c_{ij} are defined as

$$c_{11}^{(r)}=c_{22}^{(r)}=\frac{E^{(r)}(z)}{1-\left(\nu^{(r)}(z)\right)^2},c_{12}^{(r)}=\nu^{(r)}(z)c_{11}^{(r)},c_{44}^{(r)}=c_{55}^{(r)}=c_{66}^{(r)}=\frac{E^{(r)}(z)}{2\left(1+\nu^{(r)}(z)\right)}, \tag{11}$$

where $E^{(r)}(z)$ and $\nu^{(r)}(z)$ indicate the Young's modulus and Poisson's ratio of layer r, respectively.

2.3. Equilibrium Equations

The equilibrium equations can be obtained by applying the principle of total potential energy. It can be expressed in its analytical form as

$$\sum_{r=1}^{3}\int_{h_{r-1}}^{h_r}\int_\Omega\left\{\left(\sigma_i^{(r)}\delta\varepsilon_i^{(r)}+\tau_{ij}^{(r)}\delta\gamma_{ij}^{(r)}\right)\mathrm{d}z\right\}\mathrm{d}\Omega+\int_\Omega\left(S_1\frac{\partial^2 w}{\partial x^2}++S_2\frac{\partial^2 w}{\partial y^2}\right)\delta u_3\mathrm{d}\Omega=0, \tag{12}$$

where $i, j = x, y, z$, S_1 and S_2 are the membrane forces caused by in-plane end loads, and h_r and h_{r-1} (r = 1, 2, 3) are the top and bottom z-coordinates of the rth layer. By inserting Equations (7) and (8) into Equation (12), this yields

$$\begin{array}{c}\sum_{r=1}^{3}\int_{h_{r-1}}^{h_r}\int_{\Omega}\Big\{\sigma_x^{(r)}\Big(\frac{\partial\delta u}{\partial x}-z\frac{\partial^2\delta w}{\partial x^2}+\varphi(z)\frac{\partial\delta\theta_x}{\partial x}\Big)+\sigma_y^{(r)}\Big(\frac{\partial\delta v}{\partial y}-z\frac{\partial^2\delta w}{\partial y^2}+\varphi(z)\frac{\partial\delta\theta_y}{\partial y}\Big)\\ +\sigma_z^{(r)}(\varphi''(z)\delta\theta_z)+\tau_{yz}^{(r)}\Big[\frac{\partial\delta v}{\partial x}+\frac{\partial\delta u}{\partial y}-2z\frac{\partial^2\delta w}{\partial x\partial y}+\varphi(z)\Big(\frac{\partial\delta\theta_x}{\partial y}+\frac{\partial\delta\theta_y}{\partial x}\Big)\Big]\\ +\tau_{xz}^{(r)}\Big[\varphi'(z)\Big(\delta\theta_x+\frac{\partial\delta\theta_z}{\partial x}\Big)\Big]+\tau_{yz}^{(r)}\Big[\varphi'(z)\Big(\delta\theta_y+\frac{\partial\delta\theta_z}{\theta y}\Big)\Big]\Big\}\mathrm{d}z\mathrm{d}\Omega\\ +\int_{\Omega}\Big(S_1\frac{\partial^2 w}{\partial x^2}++S_2\frac{\partial^2 w}{\partial y^2}\Big)\delta u_3\mathrm{d}\Omega=0\end{array} \tag{13}$$

When integrating Equation (13) in parts, the following are obtained:

$$\begin{array}{c}-\int_{\Omega}\Big\{\Big(\frac{\partial N_x}{\partial x}+\frac{\partial N_{xy}}{\partial y}\Big)\delta u+\Big(\frac{\partial N_{xy}}{\partial x}+\frac{\partial N_y}{\partial y}\Big)\delta v+\Big(\frac{\partial^2 M_x}{\partial x^2}+2\frac{\partial^2 M_{xy}}{\partial x\partial y}+\frac{\partial^2 M_y}{\partial y^2}\Big)\delta w\\ +\Big(\frac{\partial P_x}{\partial x}+\frac{\partial P_{xy}}{\partial y}-Q_{xz}\Big)\delta\theta_x+\Big(\frac{\partial P_{xy}}{\partial x}+\frac{\partial P_y}{\partial y}-Q_{xz}\Big)\delta\theta_y+\Big(\frac{\partial Q_{xy}}{\partial x}+\frac{\partial Q_{yz}}{\partial y}-N_z\Big)\delta\theta_z\\ +\Big(S_1\frac{\partial^2 w}{\partial x^2}+S_2\frac{\partial^2 w}{\partial y^2}\Big)\delta w\Big\}\mathrm{d}\Omega=0,\end{array} \tag{14}$$

where N_i, M_i, P_i, and Q_j ($i = x,\ y,\ xy$, $j = xz,\ yz$) are the resultant stress, moment, additional stress couples, and transverse shear stress resultants, respectively. The equilibrium equations are determined from Equation (14) by setting the coefficients of δu, δv, δw, $\delta\theta_x$, $\delta\theta_y$, and $\delta\theta_z$ to zero separately. Then, the equilibrium equations of the current theory are obtained as

$$\begin{array}{c}\delta u:\frac{\partial N_x}{\partial x}+\frac{\partial N_{xy}}{\partial y}=0,\ \delta v:\frac{\partial N_{xy}}{\partial x}+\frac{\partial N_y}{\partial y}=0,\\ \delta w:\frac{\partial^2 M_x}{\partial x^2}+2\frac{\partial^2 M_{xy}}{\partial x\partial y}+\frac{\delta^2 M_y}{\delta y^2}+S1\frac{\partial^2 w}{\partial x^2}+S2\frac{\partial^2 w}{\partial y^2}=0,\ \delta\theta_x:\frac{\partial P_x}{\partial x}+\frac{\partial P_{xy}}{\partial y}-Q_{xz}=0,\\ \delta\theta_y:\frac{\partial P_{xy}}{\partial x}+\frac{\partial P_y}{\partial y}-Q_{yz}=0,\ \delta\theta_z:\frac{\partial Q_{xy}}{\partial x}+\frac{\partial Q_{yz}}{\partial y}-N_z=0.\end{array} \tag{15}$$

where

$$\begin{array}{c}\{N_{ij},M_{ij},P_{ij}\}=\sum_{r=1}^{3}\int_{h_{r-1}}^{h_r}\sigma_{ij}^{(r)}\{1,z,\varphi(z)\}\mathrm{d}z,\ Q_{iz}=\sum_{r=1}^{3}\int_{h_{r-1}}^{h_r}\sigma_{iz}^{(r)}\varphi'(z)\mathrm{d}z\\ N_z=\sum_{r=1}^{3}\int_{h_{r-1}}^{h_r}\sigma_z^{(r)}\ \varphi''(\mathrm{z})\ \mathrm{dz},\ (i,j=x,y).\end{array} \tag{16}$$

Substituting Equation (9) into Equation (16) via integration across the thickness yields the following:

$$\left\{\begin{array}{c}N_x\\N_y\\M_x\\M_y\\P_x\\P_y\\N_z\end{array}\right\}=\left[\begin{array}{ccccccc}A_{11}&A_{12}&B_{11}&B_{12}&B_{11}^*&B_{12}^*&G_{13}^*\\A_{12}&A_{22}&B_{12}&B_{22}&B_{12}^*&B_{22}^*&G_{23}^*\\B_{11}&B_{12}&D_{11}&D_{12}&D_{11}^*&D_{12}^*&H_{13}^*\\B_{12}&B_{22}&D_{12}&D_{22}&D_{12}^*&D_{22}^*&H_{23}^*\\B_{11}^*&B_{12}^*&D_{11}^*&D_{12}^*&F_{11}^*&F_{12}^*&L_{13}^*\\B_{12}^*&B_{22}^*&D_{12}^*&D_{22}^*&F_{12}^*&F_{22}^*&L_{23}^*\\G_{13}^*&G_{23}^*&H_{11}^*&H_{23}^*&L_{13}^*&L_{23}^*&J_{33}^*\end{array}\right]\left\{\begin{array}{c}\varepsilon_x^0\\\varepsilon_y^0\\\varepsilon_x^1\\\varepsilon_y^1\\\varepsilon_x^2\\\varepsilon_y^2\\\varepsilon_x^z\end{array}\right\} \tag{17}$$

$$\left\{\begin{array}{c}N_{xy}\\M_{xy}\\P_{xy}\end{array}\right\}=\left[\begin{array}{ccc}A_{66}&B_{66}&B_{66}^*\\B_{66}&D_{66}&D_{66}^*\\B_{66}^*&D_{66}^*&F_{66}^*\end{array}\right]\left\{\begin{array}{c}\gamma_{xy}^0\\\gamma_{xy}^1\\\gamma_{xy}^2\end{array}\right\},\left\{\begin{array}{c}Q_{yz}\\Q_{xz}\end{array}\right\}\left[\begin{array}{cc}J_{44}^*&0\\0&J_{55}^*\end{array}\right]\left\{\begin{array}{c}\gamma_{yz}^0\\\gamma_{xz}^0\end{array}\right\},$$

where the plate stiffnesses are expressed as

$$\begin{array}{l}\left\{A_{ij}, B_{ij}, D_{ij}\right\} = \sum_{r=1}^{3} \int_{h_{r-1}}^{h_r} c_{ij}^{(r)} \left\{1, z, z^2\right\} \mathrm{d}z,\ ij = 1, 2, 6, \\ \left\{B_{ij}^*, D_{ij}^*, F_{ij}^*\right\} = \sum_{r=1}^{3} \int_{h_{r-1}}^{h_r} c_{ij}^{(r)} \varphi(z) \{1, z, \varphi(z)\} \mathrm{d}z, \\ \left\{G_{r3}^*, H_{r3}^*, L_{r3}^*\right\} = \sum_{r=1}^{3} \int_{h_{r-1}}^{h_r} c_{ij}^{(r)} \varphi''(z) \{1, z, \varphi(z)\} \mathrm{d}z,\ r = 1, 2, \\ J_{\tau\tau}^* = \sum_{r=1}^{3} \int_{h_{r-1}}^{h_r} c_{\tau\tau}^{(r)} \left(\varphi'(z)\right)^2 \mathrm{d}z,\ \tau = 4, 5.\end{array} \tag{18}$$

The equilibrium equations can be expressed in terms of displacement as

$$\begin{array}{c} A_{11}\frac{\partial^2 u}{\partial x^2} + A_{66}\frac{\partial^2 u}{\partial y^2} + (A_{12} + A_{66})\frac{\partial^2 v}{\partial x \partial y} - B_{11}\frac{\partial^3 w}{\partial x^3} - (B_{12} + 2B_{66})\frac{\partial^3 w}{\partial x \partial y^2} + \\ A_{11}^*\frac{\partial^2 \theta_x}{\partial x^2} + A_{66}^*\frac{\partial^2 \theta_y}{\partial y^2} + \left(A_{12}^* + A_{66}^*\right)\frac{\partial^2 \theta_y}{\partial x \partial y} - G_{13}^*\frac{\partial \theta_z}{\partial x} = 0, \\ (A_{12} + A_{66})\frac{\partial^2 u}{\partial x \partial y} + A_{66}\frac{\partial^2 v}{\partial x^2} + A_{11}\frac{\partial^2 v}{\partial y^2} - (B_{12} + 2B_{66})\frac{\partial^3 w}{\partial x^2 \partial y} - B_{11}\frac{\partial^3 w}{\partial y^3} + \\ A_{66}^*\frac{\partial^2 \theta_x}{\partial x^2} + A_{11}^*\frac{\partial^2 \theta_y}{\partial y^2} + \left(A_{12}^* + A_{66}^*\right)\frac{\partial^2 \theta_x}{\partial x \partial y} - G_{23}^*\frac{\partial \theta_z}{\partial y} = 0, \\ B_{11}\frac{\partial^3 u}{\partial x^3} + (B_{12} + 2B_{66})\frac{\partial^3 u}{\partial x \partial y^2} + (B_{12} + 2B_{66})\frac{\partial^3 v}{\partial x^2 \partial y} + B_{11}\frac{\partial^3 v}{\partial y^3} - \\ D_{11}\frac{\partial^4 w}{\partial x^4} - D_{11}\frac{\partial^4 w}{\partial x^2 \partial y^2} - D_{22}\frac{\partial^4 w}{\partial y^4} - \left(S^E + S^b\right)\left(\frac{\partial^2 w}{\partial x^2} + \frac{\partial^2 w}{\partial y^2}\right) + D_{11}^*\frac{\partial^3 \theta_x}{\partial x^3} + \\ \left(D_{12}^* + 2D_{66}^*\right)\frac{\partial^3 \theta_x}{\partial x^2 \partial y} + D_{11}^*\frac{\partial^3 \theta_y}{\partial y^3} + \left(D_{12}^* + 2D_{66}^*\right)\frac{\partial^3 \theta_y}{\partial x^2 \partial y} + H_{13}^*\frac{\partial^2 \theta_z}{\partial x^2} + H_{23}^*\frac{\partial^2 \theta_z}{\partial y^2} = 0, \\ B_{11}^*\frac{\partial^2 u}{\partial x^2} + B_{66}^*\frac{\partial^2 u}{\partial y^2} + \left(B_{12}^* + B_{66}^*\right)\frac{\partial^2 v}{\partial x \partial y} - D_{11}^*\frac{\partial^3 w}{\partial x^3} - \left(D_{12}^* + 2D_{66}^*\right)\frac{\partial^3 w}{\partial x^2 \partial y} - \\ J_{55}^*\theta_x + F_{11}^*\frac{\partial^2 \theta_x}{\partial x^2} + F_{66}^*\frac{\partial^2 \theta_x}{\partial y^2} + \left(F_{12}^* + F_{66}^*\right)\frac{\partial^2 \theta_y}{\partial x \partial y} + \left(J_{55}^* - L_{13}^*\right)\frac{\partial \theta_z}{\partial x} = 0, \\ \left(B_{12}^* + B_{66}^*\right)\frac{\partial^2 u}{\partial x \partial y} + B_{66}^*\frac{\partial^2 v}{\partial x^2} + B_{22}^*\frac{\partial^2 v}{\partial y^2} - D_{22}^*\frac{\partial^3 w}{\partial y^3} - \left(D_{12}^* + 2D_{66}^*\right)\frac{\partial^3 w}{\partial x^2 \partial y} + \\ \left(F_{12}^* + F_{66}^*\right)\frac{\partial^2 \theta_x}{\partial x \partial y} + J_{44}^* + F_{66}^*\frac{\partial^2 \theta_y}{\partial x^2} + F_{22}^*\frac{\partial^2 \theta_y}{\partial y^2} + \left(J_{44}^* - L_{23}^*\right)\frac{\partial \theta_z}{\partial y} = 0, \\ -G_{13}^*\frac{\partial u}{\partial x} - G_{23}^*\frac{\partial v}{\partial y} + H_{13}^*\frac{\partial^2 \mathrm{w}}{\partial x^2} + H_{23}^*\frac{\partial^2 \mathrm{w}}{\partial y^2} + \left(J_{55}^* - L_{13}^*\right)\frac{\partial \theta_x}{\partial x} + \left(J_{44}^* - L_{23}^*\right)\frac{\partial \theta_y}{\partial y} \\ + J_{33}^*\theta_z + J_{55}^*\frac{\partial^2 \theta_z}{\partial x^2} + J_{44}^*\frac{\partial^2 \theta_z}{\partial y^2} = 0. \end{array} \tag{19}$$

3. Closed-Form Solution

Navier's procedure is used to derive the exact solution of the mechanical buckling problem. The following boundary conditions are required at the side edges to apply this method:

$$\begin{array}{c} v = w = \theta_y = \theta_z = N_x = M_x = P_x = 0 \text{ at } x = 0,\ a, \\ u = w = \theta_x = \theta_z = N_y = M_y = P_y = 0 \text{ at } y = 0,\ b. \end{array} \tag{20}$$

The forms of the displacement expressions that are assumed to satisfy the boundary conditions are defined as

$$\left\{\begin{array}{c}(u, \theta_x) \\ (v, \theta_y) \\ (w, \theta_z)\end{array}\right\} = \left\{\begin{array}{c}(U, X)\cos(\lambda_m x)\sin(\mu_n y) \\ (V, Y)\sin(\lambda_m x)\cos(\mu_n y) \\ (W, Z)\sin(\lambda_m x)\sin(\mu_n y)\end{array}\right\}, \tag{21}$$

where $\lambda_m = \frac{m\pi}{a}$, $\mu_n = \frac{n\pi}{b}$, m, and n are mode numbers and U, V, W, X, Y, and Z are arbitrary parameters to be determined by substituting Equation (21) into Equation (19). Then, the following analytical solution is obtained:

$$[\Gamma]\{\Lambda\} = \{0\}, \tag{22}$$

where

$$\{\Lambda\} = \{U,\ V,\ W,\ X,\ Y, Z\}^t, \tag{23}$$

The components $\Gamma_{ij} = \Gamma_{ji}$ of the matrix $[\Gamma]$ are expressed as

$$\begin{gathered}
\Gamma_{11} = -\lambda_m^2 A_{11} - \mu_n^2 A_{66}, \Gamma_{12} = -\lambda_m \mu_n\ (A_{12} + A_{66}),\\
\Gamma_{13} = \lambda_m^3 B_{11} + \lambda_m \mu_n^2\ (B_{12} + 2B_{66}),\ \ \Gamma_{14} = -\lambda_m^2 B_{11}^* - \mu_n^2 B_{66}^*,\\
\Gamma_{15} = -\lambda_m \mu_n \left(B_{12}^* + B_{66}^*\right), \Gamma_{16} = \lambda_m G_{13}^*,\ \ \Gamma_{22} = -\lambda_m^2 A_{66} - \mu_n^2 A_{22},\\
\Gamma_{23} = \mu_n^3 B_{22} + \lambda_m^2 \mu_n (B_{12} + 2B_{66}),\ \ \Gamma_{24} = -\lambda_m \mu_n\ \left(B_{12}^* + B_{66}^*\right),\\
\Gamma_{25} = -\lambda_m^2 B_{66}^* - \mu_n^2 B_{22}^*, \Gamma_{26} = \mu_n G_{23}^*,\\
\Gamma_{33} = \lambda_m^4 D_{11} + 2\lambda_m^2 \mu_n^2\ (D_{12} + 2D_{66}) + \mu_m^4 D_{22} - \lambda_m^2 S_1 - \mu_n^2 S_2,\\
\Gamma_{34} = -\lambda_m^3 D_{11}^* - \lambda_m \mu_n^2\ \left(D_{12}^* + 2D_{66}^*\right), \Gamma_{35} = -\mu_n^3 D_{22}^* - \lambda_m^2 \mu_n\ \left(D_{12}^* + 2D_{66}^*\right),\\
\Gamma_{36} = \lambda_m^2 H_{13}^* + \mu_n^2 H_{23}^*, \Gamma_{44} = -J_{55}^* - \lambda_m^2 F_{11}^* - \mu_n^2 F_{66}^*,\\
\Gamma_{45} = -\lambda_m \mu_n \left(F_{12}^* + F_{66}^*\right), \Gamma_{46} = \lambda_m \left(L_{13}^* - J_{55}^*\right),\ \ \Gamma_{55} = -J_{44}^* - \lambda_m^2 F_{66}^* - \mu_n^2 F_{22}^*,\\
\Gamma_{56} = \mu_n \left(L_{23}^* - J_{44}^*\right),\ \ \Gamma_{66} = J_{33}^* + \lambda_m^2 J_{55}^* + \mu_n^2 J_{44}^*.
\end{gathered} \tag{24}$$

4. Numerical Results and Discussions

The buckling response of simply supported FG porous plates with several configurations subject to various loading conditions is presented. In these results, the shear and normal strain were considered. The porous plate was made of alumina (Al_2O_3) as the ceramic and aluminum (Al) as the metal. The plate material properties of the FG layer were graded across the z direction, where the top surface was fully ceramic while the bottom surface was fully metal. The elasticity modulus of alumina is E_c =380 GPa, and aluminum's is $E_m = 70$ GPa, while Poisson's ratio is $\nu = 0.3$. In this analysis, $N_{cr} = S_1$ and $S_2 = \gamma\ S_1$, where γ is the in-plane loadings, which are uniaxial compression ($\gamma = 0$) and biaxial compression ($\gamma = 1$).

4.1. FG Porous Plates

The critical buckling of isotropic FG porous plates for various volume fraction exponents k, aspect ratio a/b, and side-to-thickness ratio a/h are presented in Tables 1 and 2. The present porous plate describes the variation of the materials based on a modified polynomial law. The obtained results were calculated for two in-plane loads cases: uniaxial compression ($\gamma = 0$) and biaxial compression ($\gamma = 1$). The inclusion of porosity was considered in this investigation. The critical buckling was determined based on the following dimensionless parameter [6,44–46]:

$$\widetilde{N}_{cr} = \frac{N_{cr}\ a^2}{E_m h^3}. \tag{25}$$

Table 1. The critical buckling loads $\widetilde{N}_{cr}$ of isotropic FG porous plates ($\gamma = 0$, Model I).

a/b	*a/h*	**Theory**		ε_z	***k***					
					0	**0.5**	**1**	**2**	**5**	**10**
0.5	5	Present	$\xi = 0.1$	$\neq 0$	6.43352	4.10285	3.06133	2.23716	1.71195	1.49599
			$\xi = 0$	$\neq 0$	6.96910	4.63564	3.62143	2.82963	2.28633	2.02068
				$= 0$	6.72084	4.42374	3.41659	2.64599	2.15129	1.92284
		RSDT [6]		$\neq 0$	6.963	4.630	3.618	2.830	2.283	2.018
		HSDT [44]		$= 0$	6.714	4.409	3.39	2.61	2.124	1.90
		RSDT [45]		$= 0$	6.7203	4.4235	3.4164	2.6451	2.1484	1.9213

Table 1. *Cont.*

a/b	*a/h*	Theory		ε_z	*k*					
					0	**0.5**	**1**	**2**	**5**	**10**
0.5	10	Present	$\xi = 0.1$	$\neq 0$	6.91620	4.36526	3.25199	2.39253	1.89252	1.68723
			$\xi = 0$	$\neq 0$	7.49362	4.93859	3.85845	2.82963	2.53365	2.26485
				$= 0$	7.40554	4.82073	3.71118	2.88994	2.41739	2.19013
		RSDT [6]		$\neq 0$	7.480	4.928	3.852	3.041	2.530	2.259
		HSDT [44]		$= 0$	7.397	4.81	3.70	2.87	2.40	2.18
		RSDT [45]		$= 0$	7.405	4.82	3.71	2.88	2.41	2.18
1	5	Present	$\xi = 0.1$	$\neq 0$	15.57565	10.00664	7.47646	5.43900	4.06881	3.50879
			$\xi = 0$	$\neq 0$	16.87004	11.29550	8.82513	6.85195	5.42442	4.75810
				$= 0$	16.02248	10.62598	8.22513	6.34613	5.06271	4.48574
		RSDT [6]		$\neq 0$	16.866	11.288	8.823	6.855	5.418	4.755
		HSDT [44]		$= 0$	16.00	10.57	8.146	6.23	4.97	4.44
		RSDT [45]		$= 0$	16.02	10.62	8.22	6.34	5.05	4.48
	10	Present	$\xi = 0.1$	$\neq 0$	17.44699	11.03593	8.22396	6.04171	4.74522	4.21204
			$\xi = 0$	$\neq 0$	18.90267	12.48193	9.75157	7.67526	6.34950	5.66185
				$= 0$	18.57932	12.12331	9.33944	7.26418	6.03894	5.45491
		RSDT [6]		$\neq 0$	18.873	12.459	9.738	7.673	6.341	5.650
		HSDT [44]		$= 0$	18.54	12.08	9.299	7.21	5.99	5.42
		RSDT [45]		$= 0$	18.57	12.12	9.33	7.26	6.03	5.45

Table 2. The critical buckling loads $\widetilde{N}_{cr}$ of isotropic FG porous plate ($\gamma = 1$, Model I).

a/b	*a/h*	Theory		ε_z	*k*					
					0	**0.5**	**1**	**2**	**5**	**10**
0.5	5	Present	$\xi = 0.1$	$\neq 0$	5.14681	3.28228	2.44907	1.78973	1.36956	1.19679
			$\xi = 0$	$\neq 0$	5.57528	3.70851	2.89714	2.26371	1.82906	1.61654
				$= 0$	5.37667	3.53899	2.73327	2.11679	1.72103	1.53827
		RSDT [6]		$\neq 0$	5.570	3.704	2.895	2.264	1.826	1.614
		HSDT [46]		$\neq 0$	5.4090	3.5652	2.7563	2.1348	1.7320	1.5474
		RSDT [45]		$= 0$	5.376	3.539	2.733	2.116	1.719	1.537
	10	Present	$\xi = 0.1$	$\neq 0$	5.53296	3.49221	2.60159	1.91402	1.51402	1.34978
			$\xi = 0$	$\neq 0$	5.99490	3.95087	3.08676	2.43435	2.02692	1.81188
				$= 0$	5.92443	3.85658	2.96895	2.31195	1.93391	1.75211
		RSDT [6]		$\neq 0$	5.984	3.942	3.082	2.433	2.024	1.807
		HSDT [46]		$\neq 0$	5.9343	3.8644	2.9758	2.3174	1.9374	1.7551
		RSDT [45]		$= 0$	5.926	3.857	2.969	2.312	1.933	1.752

Table 2. *Cont.*

a/b	*a/h*	Theory		ε_z	*k*					
					0	**0.5**	**1**	**2**	**5**	**10**
1	5	Present	$\xi = 0.1$	$\neq 0$	7.78782	5.00332	3.73823	2.71950	2.03440	1.75439
			$\xi = 0$	$\neq 0$	8.43502	5.64775	4.41256	3.42597	2.71221	2.37905
				$= 0$	8.01124	5.31299	4.11256	3.17306	2.53135	2.24287
		SRSDT [6]		$\neq 0$	8.433	5.644	4.411	3.427	2.709	2.377
		HSDT [46]		$\neq 0$	8.0826	5.3716	4.1643	3.2132	2.5549	2.2621
		RSDT [45]		$= 0$	8.011	5.313	4.112	3.172	2.527	2.240
	10	Present	$\xi = 0.1$	$\neq 0$	8.72349	5.51796	4.11198	3.02085	2.37261	2.10602
			$\xi = 0$	$\neq 0$	9.45133	6.24096	4.87578	3.83763	3.17475	2.83092
				$= 0$	9.28966	6.06165	4.66972	3.63209	3.01947	2.72745
		RSDT [6]		$\neq 0$	9.436	6.229	4.869	3.836	3.170	2.825
		HSDT [46]		$\neq 0$	9.3139	6.0810	4.6867	3.6455	3.0280	2.7346
		RSDT [45]		$= 0$	9.289	6.062	4.670	3.632	3.018	2.726

The current results of isotropic FG perfect plates were compared with those determined via the refined plate theory (RSDT) of Zenkour and Aljadani [6] and Thai and Choi [45] as well as the higher-order plate theory (HSDT) of Reddy et al. [44] and Thinh et al. [46]. It can be noted that the present solutions were in excellent agreement with those reported in [6,46], as the thickness stretching was considered. However, the reported calculations in [44,45] slightly underestimated the critical buckling of thick FG plates. This was due to the neglect of the thickness stretching effect. Moreover, the critical buckling rose with the increase in the aspect ratio as well as the side-to-thickness ratio. It can be observed that the critical buckling decreased by increasing the porosity parameter. This means that the porosity inclusion on the plate structure reduced the plate stiffness, which decreased the critical buckling loads.

4.2. FG Porous Sandwich Plates

Two types of simply supported FG sandwich porous plates are presented. Model II is composed of FG porous layers at the upper and lower surfaces, while the core is a perfect ceramic, and Model III is composed of perfect homogenous layers at the upper and lower surfaces, while the core is made of FG with porosity. $h_0 = -h/2$ and $h_3 = h/2$ are the lower and upper faces. Various types of FG sandwich porous plate schemes were assumed, and they are listed below [47,48]:

- **The (1-0-1) FG Sandwich Porous Plate**

  The structure is composed of two equal skin layers, and thus

$$h_1 = h_2 = 0. \tag{26}$$

- **The (1-1-1) FG Sandwich Porous Plate**

  This plate has three equal-thickness layers, and therefore

$$h_1 = -\frac{h}{6}, h_2 = \frac{h}{6}. \tag{27}$$

- **The (1-2-1) FG Sandwich Porous Plate**

This plate has a core with double the thickness of the skin layer:

$$h_1 = -\frac{h}{4}, h_2 = \frac{h}{4}. \tag{28}$$

- **The (2-1-2) FG Sandwich Porous Plate**

The core thickness of this plate is half the thickness of the skin layer, and hence

$$h_1 = -\frac{h}{10}, h_2 = \frac{h}{10}. \tag{29}$$

- **The (2-2-1) FG Sandwich Porous Plate**

This non-symmetric sandwich porous plate has a core and lower skin layer with the same thickness as double the upper skin sheet, such that

$$h_1 = -\frac{h}{10}, h_2 = \frac{3h}{10}. \tag{30}$$

- **The (2-1-1) FG Sandwich Porous Plate**

This non-symmetric sandwich porous plate has a core and upper skin layer with the same thickness, and they are half of the lower skin layer. Therefore, the following is true:

$$h_1 = 0, h_2 = \frac{h}{4}. \tag{31}$$

- **The (1-3-1) FG Sandwich Porous Plate**

The core thickness of this plate is triple the thickness of the skin layer, and thus

$$h_1 = -\frac{3h}{10}, h_2 = \frac{3h}{10}. \tag{32}$$

In this study, the critical buckling was determined based on the following dimensionless parameter:

$$\overline{N}_{cr} = \frac{N_{cr}\, a^2}{100h^3}. \tag{33}$$

The critical buckling of FG square sandwich plates (Model II) is shown in Tables 3 and 4. The following parameters were used: $a/h = 10$ and $a/b = 1$. The sandwich plate was composed of FG porous layers at the upper and lower surfaces, while the core was a perfect ceramic. The current solutions for sandwich FG perfect plates were compared with those determined via the higher-order shear deformation plate theory of Daikh and Zenkour [27] and Zenkour [9]. It should be noted that the results of the present theory ($\varepsilon_z = 0$) agreed well with those reported in [9,27] due to ignoring the stretching effect in these results. However, the present solution ($\varepsilon_z \neq 0$) was slightly higher compared with that of [9,27]. This shows that the thickness stretching impact could affect the buckling response of sandwich FG plates. This indicates that the current theory gave more accurate results than higher-order shear deformation theories. Furthermore, the critical buckling decreased with the rise in the volume fraction exponent. The critical buckling of the sandwich FG porous plate under biaxial load had a lower value than the uniaxial buckling load for any value of the volume fraction exponent. The structure (1-2-1) had the highest buckling load among the other structures. This was because (1-2-1) had the highest volume fraction of the ceramic phase, hardening the structure.

Table 3. The critical buckling load $\overline{N}_{cr}$ of an FG square sandwich plate ($\gamma = 1$, Model II).

k	Theory	ε_z	1-0-1	1-1-1	1-2-1	2-1-2	2-2-1	2-1-1
0	Present	$\neq 0$	6.61593	6.61593	6.61593	6.61593	6.61593	6.61593
		$= 0$	6.50276	6.50276	6.50276	6.50276	6.50276	6.50276
	SHSDT [27]	$= 0$	6.50266	6.50266	6.50266	6.50266	6.50266	6.50266
	SSDT [9]	$= 0$	6.50303	6.50303	6.50303	6.50303	6.50303	6.50303
	FPT [9]	$= 0$	6.50224	6.50224	6.50224	6.50224	6.50224	6.50224
	CPT [9]	$= 0$	6.86896	6.86896	6.86896	6.86896	6.86896	6.86896
0.5	Present	$\neq 0$	3.75098	4.29737	4.69467	4.04480	4.49177	4.19455
		$= 0$	3.68189	4.21823	4.60878	3.97022	4.40514	4.11235
	SHSDT [27]	$= 0$	3.68250	4.21836	4.60832	3.97068	4.40504	4.11249
	SSDT [9]	$= 0$	3.68284	4.21856	4.60835	3.97097	4.40519	4.11269
	FPT [9]	$= 0$	3.66866	4.20517	4.59758	3.95660	4.39336	4.10007
	CPT [9]	$= 0$	3.82699	4.39032	4.80762	4.12798	4.59127	4.28112
1	Present	$\neq 0$	2.63324	3.29531	3.82615	2.97666	3.55158	3.16779
		$= 0$	2.58314	3.23224	3.75359	2.91970	3.47476	3.09685
	SHSDT [27]	$= 0$	2.58391	3.23252	3.75317	2.92032	3.47479	3.09713
	SSDT [9]	$= 0$	2.58423	3.23270	3.75314	2.92060	3.47490	3.09731
	FPT [9]	$= 0$	2.57118	3.21946	3.74182	2.90690	3.46286	3.08510
	CPT [9]	$= 0$	2.66624	3.34075	3.89203	3.01366	3.59831	3.20195
5	Present	$\neq 0$	1.35326	1.82621	2.41649	1.55090	2.11731	1.75366
		$= 0$	1.32839	1.78936	2.36731	1.52070	2.05578	1.70140
	SHSDT [27]	$= 0$	1.32960	1.79007	2.36739	1.52169	2.05625	1.70202
	SSDT [9]	$= 0$	1.33003	1.79032	2.36744	1.52203	2.05644	1.70224
	FPT [9]	$= 0$	1.31921	1.77979	2.35737	1.51126	2.04642	1.69269
	CPT [9]	$= 0$	1.36540	1.82866	2.42859	1.55352	2.10619	1.74209

Table 5 shows the porosity's impact on the critical buckling of the FG square sandwich plates (Model II). The predicted solutions were compared with the results of the higher-order shear deformation plate theory of Daikh and Zenkour [27]. It was found that the present solution ($\varepsilon_z = 0$) was in excellent agreement with the results in [27], while the obtained solutions ($\varepsilon_z \neq 0$) were in very close agreement. This work demonstrates that the thickness stretching effect had an impact on the buckling response of the sandwich FG porous plates, as ($\varepsilon_z \neq 0$) had greater critical buckling than ($\varepsilon_z = 0$). This shows that the current formulation predicted more accurate results compared with higher-order shear deformation theories. Moreover, the critical buckling reduced as the porosity parameter rose.

Tables 6 and 7 display the critical buckling of the FG square sandwich plates (Model III). The sandwich plate was composed of perfect homogenous layers at the upper and lower surfaces, while the core was FG with porosity. The achieved solutions were compared with the results associated with the inverse trigonometric shear deformation plate theory of Nguyen et al. [17]. Good agreement between the results was found when the thickness stretching effect was ignored. The critical buckling was higher when ($\varepsilon_z \neq 0$) than ($\varepsilon_z = 0$). The effect of thickness stretching appeared to be significant in the thicker plates. Still, the thickness stretching effect must always be considered in the formulation for thinner structures. Additionally, porosity inclusion decreased the critical buckling of the sandwich plates.

Table 4. The critical buckling load $\overline{N}_{cr}$ of an FG square sandwich plate ($\gamma = 0$, Model II).

k	Theory	ε_z	1-0-1	1-1-1	1-2-1	2-1-2	2-2-1	2-1-1
0	Present	$\neq 0$	13.23187	13.23187	13.23187	13.23187	13.23187	13.23187
		$= 0$	13.00552	13.00552	13.00552	13.00552	13.00552	13.00552
	SSDT [9]	$= 0$	13.00606	13.00606	13.00606	13.00606	13.00606	13.00606
	FPT [9]		13.00449	13.00449	13.00449	13.00449	13.00449	13.00449
	CPT [9]		13.73791	13.73791	13.73791	13.73791	13.73791	13.73791
0.5	Present	$\neq 0$	7.50197	8.59474	9.38935	8.08961	8.98355	8.38910
		$= 0$	7.36379	8.43646	9.21757	7.94045	8.81028	8.22471
	SSDT [9]	$= 0$	7.36568	8.43712	9.21670	7.94195	8.81037	8.22538
	FPT [9]		7.33732	8.41034	9.19517	7.91320	8.78673	8.20015
	CPT [9]		7.65398	8.78063	9.61525	8.25597	9.18254	8.56223
1	Present	$\neq 0$	5.26648	6.59063	7.65230	5.95333	7.10317	6.33559
		$= 0$	5.16629	6.46449	7.50718	5.83940	6.94952	6.19371
	SSDT [9]	$= 0$	5.16846	6.46539	7.50629	5.84119	6.94980	6.19461
	FPT [9]		5.14236	6.43892	7.48365	5.81379	6.92571	6.17020
	CPT [9]		5.33248	6.68150	7.78406	6.02733	7.19663	6.40391
5	Present	$\neq 0$	2.70653	3.65243	4.83298	3.10180	4.23463	3.50732
		$= 0$	2.65678	3.57873	4.73462	3.04141	4.11156	3.40280
	SSDT [9]	$= 0$	2.66006	3.58063	4.73488	3.04406	4.11288	3.40449
	FPT [9]		2.63842	3.55958	4.71475	3.02252	4.09285	3.38538
	CPT [9]		2.73080	3.65732	4.85717	3.10704	4.21238	3.48418

Table 5. Porosity effect on the critical buckling load $\overline{N}_{cr}$ of FG square sandwich porous plates ($a/h = 10$, $k = 2$, Model II).

γ	ξ	Theory	ε_z	1-0-1	1-1-1	1-2-1	2-1-2	2-2-1	2-1-1
1	0	Present	$\neq 0$	1.81253	2.45270	3.05374	2.12331	2.74200	2.33140
			$= 0$	1.77764	2.40403	2.99365	2.08151	2.67312	2.26987
		SHSDT [27]	$= 0$	1.77856	2.40449	2.99342	2.08228	2.67334	2.27031
	0.1	Present	$\neq 0$	1.38468	2.03504	2.67717	1.69386	2.32886	1.89483
			$= 0$	1.36172	1.99689	2.62266	1.66433	2.27238	1.84858
		SHSDT [27]	$= 0$	1.36232	1.99718	2.62234	1.66484	2.27248	1.84884
	0.2	Present	$\neq 0$	0.97393	1.63579	2.31862	1.28230	1.93035	1.47071
			$= 0$	0.95997	1.60453	2.26577	1.26181	1.88151	1.43594
		SHSDT [27]	$= 0$	0.96028	1.60465	2.26539	1.26208	1.88149	1.43604
0	0	Present	$\neq 0$	3.62507	4.90541	6.10749	4.24663	5.48401	4.66280
			$= 0$	3.55528	4.80807	5.98730	4.16303	5.34624	4.53975
	0.1	Present	$\neq 0$	2.76936	4.07009	5.35434	3.38772	4.65773	3.78966
			$= 0$	2.72345	3.99379	5.24532	3.32867	4.54476	3.69716
	0.2	Present	$\neq 0$	1.94786	3.27158	4.63724	2.56460	3.86071	2.94142
			$= 0$	1.91995	3.20907	4.53155	2.52363	3.76302	2.87188

Table 6. The critical buckling load $\overline{N}_{cr}$ of FG porous square sandwich plates ($\gamma = 1$, Model III).

a/h	Scheme	Theory		ε_z	*k*				
					0	**0.5**	**1**	**5**	**10**
5	1-1-1	Present	$\xi = 0.1$	$\neq 0$	2.1327	2.3948	2.5199	2.8165	2.9065
			$\xi = 0$	$\neq 0$	2.2325	2.4797	2.6004	2.8910	2.9801
				$= 0$	2.0416	2.2654	2.3773	2.6540	2.7402
		TSDT [17]		$= 0$	2.0513	2.2342	2.3333	2.5978	2.6834
	1-2-1	Present	$\xi = 0.1$	$\neq 0$	1.9134	2.3560	2.5556	3.0542	3.2185
			$\xi = 0$	$\neq 0$	2.0962	2.5015	2.6922	3.1764	3.3379
				$= 0$	1.9325	2.2935	2.4692	2.9317	3.0890
		TSDT [17]		$= 0$	1.9456	2.2725	2.4387	2.8964	3.0545
	2-2-1	Present	$\xi = 0.1$	$\neq 0$	2.1427	2.5897	2.8218	3.3917	3.5641
			$\xi = 0$	$\neq 0$	2.3335	2.7596	2.9821	3.5327	3.7006
				$= 0$	2.1270	2.5305	2.7443	3.2801	3.4446
		TSDT [17]		$= 0$	2.1369	2.5023	2.7056	3.2351	3.4009
10	1-1-1	Present	$\xi = 0.1$	$\neq 0$	2.4428	2.6316	2.7340	3.0082	3.0989
			$\xi = 0$	$\neq 0$	2.5376	2.7172	2.8163	3.0851	3.1749
				$= 0$	2.3524	2.5289	2.6285	2.9038	2.9964
		TSDT [17]		$= 0$	2.3508	2.5165	2.6123	2.8848	2.9773
	1-2-1	Present	$\xi = 0.1$	$\neq 0$	2.3019	2.6153	2.7839	3.2639	3.4365
			$\xi = 0$	$\neq 0$	2.4786	2.7676	2.9281	3.3920	3.5613
				$= 0$	2.3121	2.5859	2.7445	3.2191	3.3943
		TSDT [17]		$= 0$	2.3095	2.5768	2.7322	3.2063	3.3816
	2-2-1	Present	$\xi = 0.1$	$\neq 0$	2.3692	2.7992	3.0304	3.6274	3.8170
			$\xi = 0$	$\neq 0$	2.5838	2.9866	3.2059	3.7791	3.9631
				$= 0$	2.3930	2.8009	3.0259	3.6189	3.8096
		TSDT [17]		$= 0$	2.3928	2.7898	3.0116	3.6028	3.7937
100	1-1-1	Present	$\xi = 0.1$	$\neq 0$	2.5642	2.7182	2.8104	3.0741	3.1648
			$\xi = 0$	$\neq 0$	2.6555	2.8034	2.8929	3.1516	3.2413
				$= 0$	2.4773	2.6301	2.7237	2.9971	3.0920
		TSDT [17]		$= 0$	2.4773	2.6308	2.7236	2.9969	3.0918
	1-2-1	Present	$\xi = 0.1$	$\neq 0$	2.4659	2.7116	2.8658	3.3357	3.5109
			$\xi = 0$	$\neq 0$	2.6356	2.8657	3.0123	3.4657	3.6372
				$= 0$	2.4730	2.6998	2.8496	3.3269	3.5089
		TSDT [17]		$= 0$	2.4730	2.7015	2.8495	3.3268	3.5087
	2-2-1	Present	$\xi = 0.1$	$\neq 0$	2.4531	2.8733	3.1031	3.7079	3.9035
			$\xi = 0$	$\neq 0$	2.6765	3.0669	3.2837	3.8630	4.0526
				$= 0$	2.4963	2.9035	3.1322	3.7469	3.9479
		TSDT [17]		$= 0$	2.4963	2.9038	3.1320	3.7467	3.9476

Table 7. The critical buckling load $\overline{N}_{cr}$ of FG square sandwich porous plates ($\gamma = 0$, Model III).

a/h	Scheme	ξ	ε_z	*k*				
				0	**0.5**	**1**	**5**	**10**
5	1-1-1	0.1	$\neq 0$	4.2655	4.7897	5.0398	5.6331	5.8130
		0	$\neq 0$	4.4651	4.9595	5.2009	5.7820	5.9602
			$= 0$	4.0832	4.5308	4.7547	5.3081	5.4805
	1-2-1	0.1	$\neq 0$	3.8268	4.7121	5.1113	6.1085	6.4371
		0	$\neq 0$	4.1925	5.0031	5.3845	6.3528	6.6758
			$= 0$	3.8650	4.5870	4.9384	5.8634	6.1781
	2-2-1	0.1	$\neq 0$	4.2854	5.1795	5.6436	6.7834	7.1282
		0	$\neq 0$	4.6671	5.5192	5.9642	7.0655	7.4013
			$= 0$	4.2541	5.0610	5.4886	6.5603	6.8893
10	1-1-1	0.1	$\neq 0$	4.8856	5.2633	5.4681	6.0164	6.1979
		0	$\neq 0$	5.0752	5.4344	5.6326	6.1702	6.3498
			$= 0$	4.7049	5.0578	5.2571	5.8077	5.9929
	1-2-1	0.1	$\neq 0$	4.6038	5.2306	5.5678	6.5278	6.8731
		0	$\neq 0$	4.9573	5.5353	5.8562	6.7841	7.1226
			$= 0$	4.6243	5.1719	5.4891	6.4383	6.7886
	2-2-1	0.1	$\neq 0$	4.7385	5.5984	6.0609	7.2548	7.6341
		0	$\neq 0$	5.1676	5.9733	6.4118	7.5582	7.9263
			$= 0$	4.7861	5.6019	6.0518	7.2379	7.6192
100	1-1-1	0.1	$\neq 0$	5.1284	5.4364	5.6209	6.1483	6.3297
		0	$\neq 0$	5.3110	5.6068	5.7859	6.3033	6.4827
			$= 0$	4.9546	5.2603	5.4475	5.9942	6.1841
	1-2-1	0.1	$\neq 0$	4.9318	5.4232	5.7317	6.6715	7.0219
		0	$\neq 0$	5.2713	5.7315	6.0247	6.9314	7.2744
			$= 0$	4.9461	5.3996	5.6993	6.6539	7.0179
	2-2-1	0.1	$\neq 0$	4.9063	5.7466	6.2062	7.4159	7.8071
		0	$\neq 0$	5.3530	6.1339	6.5674	7.7261	8.1053
			$= 0$	4.9926	5.8071	6.2644	7.4938	7.8958

The effects of various porosity parameters, volume fraction exponents, FG configurations, aspect ratios, and side-to-thickness ratios are illustrated in Figure 2, Figure 3, Figure 4, Figure 5. The following parameters were used: $a/h = 10$, $a/b = 1$, $\gamma = 1$, and $k = 2$. Figure 2 shows the effect of the porosity parameter ξ and aspect ratio a/b on the critical buckling of FG porous plates with different configurations. The porosity inclusion on the plate reduced the critical buckling. The effect of the porosity increasing the aspect ratio was more pronounced for Model I, since the entire structure had porosity. The configuration of the FG porous plates and aspect ratio significantly impacted the porosity influence on the buckling of the FG porous plates.

The effects of the porosity parameter ξ and side-to-thickness ratio a/h on the critical buckling of the FG porous plates with different configurations are demonstrated in Figure 3. It can be seen that as the porosity parameter increased, the critical buckling of the FG porous plates for various a/h values became identical for Model I. However, the impact of the porosity and side-to-thickness ratio increasing in Model III gave different critical buckling loads. This was because Model III was stiffer than the other structures.

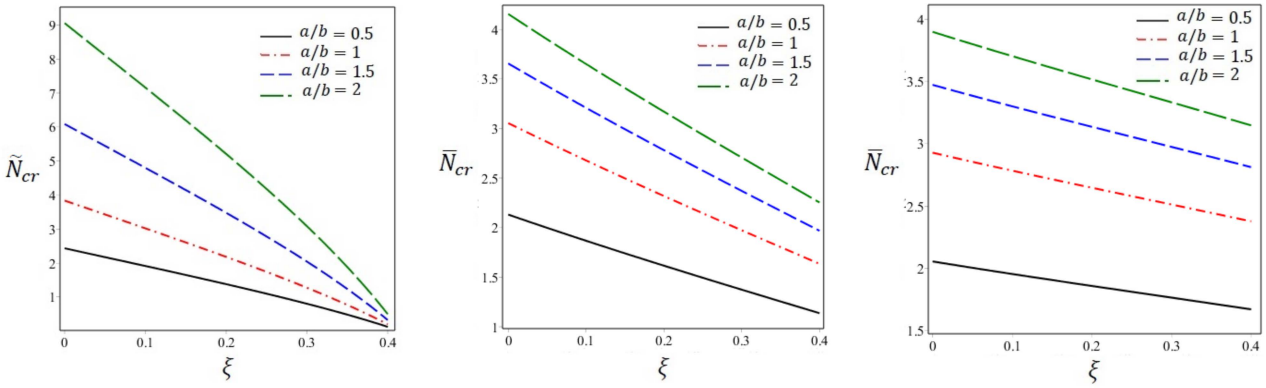

(**a**) (**b**) (**c**)

Figure 2. Porosity and aspect ratio effects on the buckling of FG porous plates ($k = 2$) for (**a**) Model I, (**b**) Model II (1-2-1), and (**c**) Model III (1-2-1).

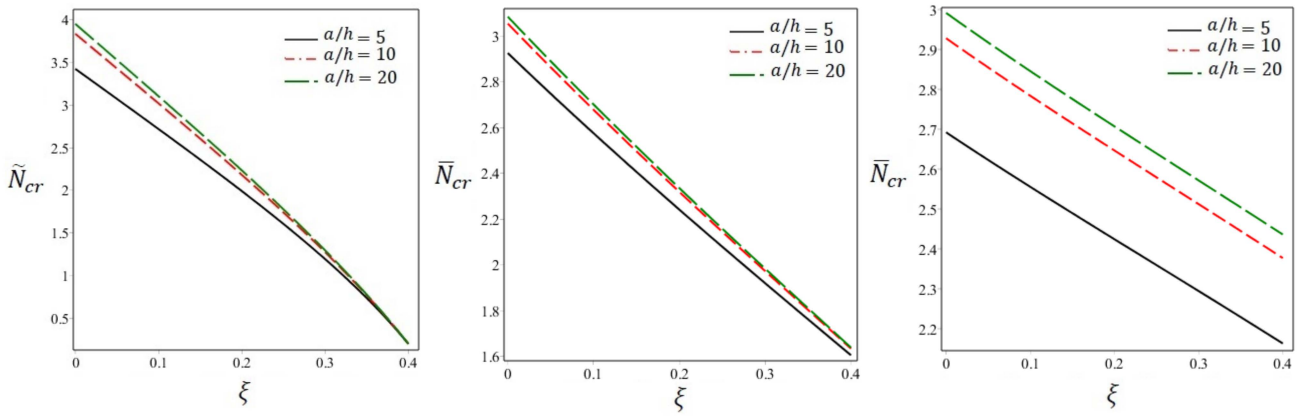

(**a**) (**b**) (**c**)

Figure 3. Porosity and side-to-thickness effects on the buckling of FG porous plates ($k = 2$) for (**a**) Model I, (**b**) Model II (1-2-1), and (**c**) Model III (1-2-1).

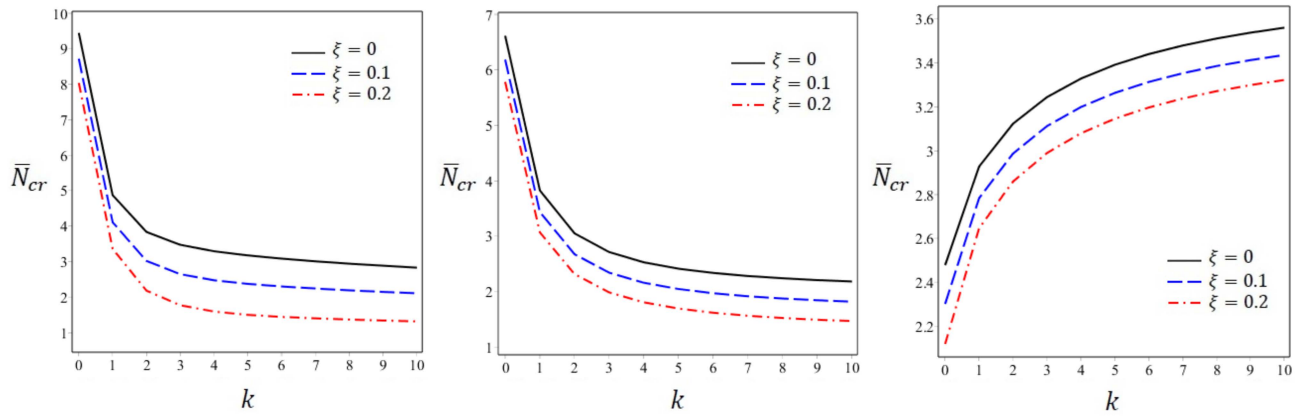

(**a**) (**b**) (**c**)

Figure 4. Porosity and volume fraction exponent effects on the buckling of FG porous plates ($k = 2$) for (**a**) Model I, (**b**) Model II (1-2-1), and (**c**) Model III (1-2-1).

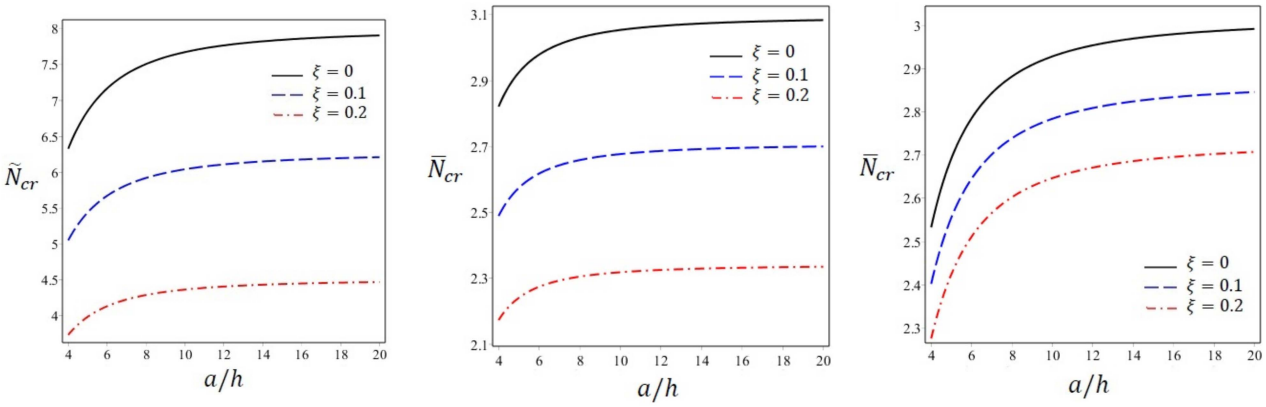

Figure 5. Porosity and side-to-thickness effects on the buckling of FG porous plates ($k = 2$) for (**a**) Model I, (**b**) Model II (1-2-1), and (**c**) Model III (1-2-1).

Figure 4 illustrates the impact of the porosity parameter and volume fraction exponent on the buckling of FG porous plates. For Models I and II, the critical buckling reduced with the rise in the volume fraction exponent. On the other hand, the critical buckling of Model III increased with the rise in the volume fraction exponent. In general, the increase of the porosity parameter reduced the plate stiffness, which decreased the critical buckling of the FG plates.

The impacts of the porosity parameters and side-to-thickness ratios on the critical buckling of the FG porous plates are presented in Figure 5. The critical buckling rose with the increase in the side-to-thickness. The impact of a/h was more significant for the FG thick plates. Moreover, the critical buckling decreased as the porosity of the plate increased. The impact of the porosity on the buckling of the porous plate increased with the rise in the side-to-thickness ratio.

5. Conclusions

This paper investigated the buckling response of FG porous plates via a quasi-3D refined theory. The thickness stretching effect was taken into consideration in this analysis. Three models of FG porous plates were considered: an isotropic FG porous plate, FG skins with a homogenous core, and an FG core with homogenous skins. Modified polynomial law was used to describe the variation in material properties. Various validation cases were presented, and calculations of a quasi-3D refined theory were presented for the FG porous plates' buckling response. Based on the presented results, the following conclusions were drawn:

- The current formulation accurately predicted the FG perfect plate buckling response compared with the higher-order shear deformation theory.
- The effect of thickness stretching appeared to be significant in the thicker plates. Still, the thickness stretching effect must always be considered in the formulation for thinner structures.
- The present results show the porosity's effect on reducing the stiffness of the plate, which decreased the critical buckling of the FG plate.
- The impact of the porosity on the buckling of the porous plate increased with the rise in the side-to-thickness ratio.
- The FG porous plates' configuration and aspect ratio significantly affected the porosity's impact on the buckling of FG porous plates.
- The critical buckling of FG porous plates under biaxial load had a lower value than a uniaxial buckling load for any value of the volume fraction exponent, side-to-thickness ratio, or porosity parameter.
- In Models I and II, the critical buckling decreased with the rise in the volume fraction exponent. On the other hand, the critical buckling of Model III increased with the

increase in the volume fraction exponent, which made the structure more reliable than the other forms.
- Among Model II's configurations, the structure (1-2-1) had the highest buckling load among the other structures.

Author Contributions: Conceptualization, A.M.Z. and M.H.A.; methodology, A.M.Z. and M.H.A.; software, M.H.A.; validation, M.H.A.; formal analysis, A.M.Z. and M.H.A.; investigation, A.M.Z.; writing—original draft preparation, M.H.A.; writing—review and editing, A.M.Z. and M.H.A.; visualization, M.H.A.; supervision, A.M.Z.; project administration, A.M.Z.; funding acquisition, A.M.Z. and M.H.A. All authors have read and agreed to the published version of the manuscript.

Funding: This research was funded by the Deanship of Scientific Research (DSR) King Abdulaziz University Jeddah under Grant No. (DG-16-130-1441).

Data Availability Statement: Not applicable.

Acknowledgments: This project was supported by the Deanship of Scientific Research (DSR), King Abdulaziz University, Jeddah, under grant No. (DG-16-130-1441). The authors, therefore, gratefully acknowledge the DSR technical and financial support.

Conflicts of Interest: The authors declare no conflict of interest, and the funders had no role in the design of the study; in the collection, analyses, or interpretation of data; in the writing of the manuscript, or in the decision to publish the results.

References

1. Daouadji, T.H.; Adim, B. An analytical approach for buckling of functionally graded plates. *Adv. Mater. Res.* **2016**, *5*, 141. [CrossRef]
2. Shariat, B.S.; Eslami, M. Buckling of thick functionally graded plates under mechanical and thermal loads. *Compos. Struct.* **2007**, *78*, 433–439. [CrossRef]
3. Liu, Z.; Wang, C.; Duan, G.; Tan, J. A new refined plate theory with isogeometric approach for the static and buckling analysis of functionally graded plates. *Int. J. Mech. Sci.* **2019**, *161*, 105036. [CrossRef]
4. Bellifa, H.; Bakora, A.; Tounsi, A.; Bousahla, A.A.; Mahmoud, S. An efficient and simple four variable refined plate theory for buckling analysis of functionally graded plates. *Steel Compos. Struct.* **2017**, *25*, 257–270.
5. Parida, S.; Mohanty, S.C. Free vibration and buckling analysis of functionally graded plates resting on elastic foundation using higher order theory. *Int. J. Struct. Stab. Dyn.* **2018**, *18*, 1850049. [CrossRef]
6. Zenkour, A.; Aljadani, M. Mechanical buckling of functionally graded plates using a refined higher-order shear and normal deformation plate theory. *Adv. Aircr. Spacecr. Sci.* **2018**, *5*, 615.
7. Sharifan, M.H.; Jabbari, M. Mechanical buckling analysis of saturated porous functionally graded elliptical plates subjected to in-plane force resting on two parameters elastic foundation based on hsdt. *J. Press. Vessel Technol.* **2020**, *142*, 041302. [CrossRef]
8. Khorasani, M.; Elahi, H.; Eugeni, M.; Lampani, L.; Civalek, O. Vibration of FG Porous Three-Layered Beams Equipped by Agglomerated Nanocomposite Patches Resting on Vlasov's Foundation. *Transp. Porous Media* In press. **2021**. [CrossRef]
9. Zenkour, A. A comprehensive analysis of functionally graded sandwich plates: Part 2—Buckling and free vibration. *Int. J. Solids Struct.* **2005**, *42*, 5243–5258. [CrossRef]
10. Neves, A.; Ferreira, A.; Carrera, E.; Cinefra, M.; Roque, C.; Jorge, R.; Soares, C.M. Static, free vibration and buckling analysis of isotropic and sandwich functionally graded plates using a quasi-3D higher-order shear deformation theory and a meshless technique. *Compos. Part B Eng.* **2013**, *44*, 657–674. [CrossRef]
11. Nguyen, T.-K.; Vo, T.P.; Thai, H.-T. Vibration and buckling analysis of functionally graded sandwich plates with improved transverse shear stiffness based on the first-order shear deformation theory. *Proc. Inst. Mech. Eng. Part C J. Mech. Eng. Sci.* **2014**, *228*, 2110–2131. [CrossRef]
12. Mantari, J.; Monge, J. Buckling, free vibration and bending analysis of functionally graded sandwich plates based on an optimized hyperbolic unified formulation. *Int. J. Mech. Sci.* **2016**, *119*, 170–186. [CrossRef]
13. Nguyen, K.; Thai, H.-T.; Vo, T. A refined higher-order shear deformation theory for bending, vibration and buckling analysis of functionally graded sandwich plates. *Steel Compos. Struct.* **2015**, *18*, 91–120. [CrossRef]
14. Neves, A.; Ferreira, A.; Carrera, E.; Cinefra, M.; Jorge, R.; Soares, C. Buckling analysis of sandwich plates with functionally graded skins using a new quasi-3D hyperbolic sine shear deformation theory and collocation with radial basis functions. *ZAMM-J. Appl. Math. Mech./Z. Angew. Math. Mech.* **2012**, *92*, 749–766. [CrossRef]
15. Akavci, S.S. Mechanical behavior of functionally graded sandwich plates on elastic foundation. *Compos. Part B Eng.* **2016**, *96*, 136–152. [CrossRef]
16. Tounsi, A.; Houari, M.S.A.; Bessaim, A. A new 3-unknowns non-polynomial plate theory for buckling and vibration of functionally graded sandwich plate. *Struct. Eng. Mech.* **2016**, *60*, 547–565. [CrossRef]

17. Nguyen, V.-H.; Nguyen, T.-K.; Thai, H.-T.; Vo, T.P. A new inverse trigonometric shear deformation theory for isotropic and functionally graded sandwich plates. *Compos. Part B Eng.* **2014**, *66*, 233–246. [CrossRef]
18. Zhu, J.; Lai, Z.; Yin, Z.; Jeon, J.; Lee, S. Fabrication of ZrO_2–NiCr functionally graded material by powder metallurgy. *Mater. Chem. Phys.* **2001**, *68*, 130–135. [CrossRef]
19. Masjedi, P.K.; Maheri, A.; Weaver, P.M. Large deflection of functionally graded porous beams based on a geometrically exact theory with a fully intrinsic formulation. *Appl. Math. Model.* **2019**, *76*, 938–957. [CrossRef]
20. Mota, A.F.; Loja, M.A.R.; Barbosa, J.I.; Rodrigues, J.A. Porous Functionally Graded Plates: An Assessment of the Influence of Shear Correction Factor on Static Behavior. *Math. Comput. Appl.* **2020**, *25*, 25. [CrossRef]
21. Kumar, R.; Lal, A.; Singh, B.; Singh, J. Meshfree approach on buckling and free vibration analysis of porous FGM plate with proposed IHHSDT resting on the foundation. *Curved Layer. Struct.* **2019**, *6*, 192–211. [CrossRef]
22. Dhuria, M.; Grover, N.; Goyal, K. Influence of porosity distribution on static and buckling responses of porous functionally graded plates. *Structures* **2021**, *34*, 1458–1474.
23. Fan, F.; Safaei, B.; Sahmani, S. Buckling and postbuckling response of nonlocal strain gradient porous functionally graded micro/nano-plates via NURBS-based isogeometric analysis. *Thin-Walled Struct.* **2021**, *159*, 107231. [CrossRef]
24. Babaei, H.; Jabbari, M.; Eslami, M.R. The effect of porosity on elastic stability of toroidal shell segments made of saturated porous functionally graded materials. *J. Press. Vessel Technol.* **2021**, *143*, 031501. [CrossRef] [PubMed]
25. Tran, T.T.; Tran, V.K.; Pham, Q.-H.; Zenkour, A.M. Extended four-unknown higher-order shear deformation nonlocal theory for bending, buckling and free vibration of functionally graded porous nanoshell resting on elastic foundation. *Compos. Struct.* **2021**, *264*, 113737. [CrossRef]
26. Thom, D.V.; Zenkour, A.M.; Doan, D.H. Buckling of cracked FG plate resting on elastic foundation considering the effect of delamination phenomenon. *Compos. Struct.* **2021**, *273*, 114278. [CrossRef]
27. Daikh, A.A.; Zenkour, A.M. Free vibration and buckling of porous power-law and sigmoid functionally graded sandwich plates using a simple higher-order shear deformation theory. *Mater. Res. Express* **2019**, *6*, 115707. [CrossRef]
28. Chen, D.; Yang, J.; Kitipornchai, S. Buckling and bending analyses of a novel functionally graded porous plate using Chebyshev-Ritz method. *Arch. Civ. Mech. Eng.* **2019**, *19*, 157–170. [CrossRef]
29. Xu, K.; Yuan, Y.; Li, M. Buckling behavior of functionally graded porous plates integrated with laminated composite faces sheets. *Steel Compos. Struct.* **2019**, *32*, 633–642.
30. Singh, S.; Harsha, S. Analysis of porosity effect on free vibration and buckling responses for sandwich sigmoid function based functionally graded material plate resting on Pasternak foundation using Galerkin Vlasov's method. *J. Sandw. Struct. Mater.* **2020**, *23*(5), 1717–1760. [CrossRef]
31. Mojahedin, A.; Jabbari, M.; Khorshidvand, A.; Eslami, M. Buckling analysis of functionally graded circular plates made of saturated porous materials based on higher order shear deformation theory. *Thin-Walled Struct.* **2016**, *99*, 83–90. [CrossRef]
32. Yang, J.; Chen, D.; Kitipornchai, S. Buckling and free vibration analyses of functionally graded graphene reinforced porous nanocomposite plates based on Chebyshev-Ritz method. *Compos. Struct.* **2018**, *193*, 281–294. [CrossRef]
33. Vo, T.P.; Thai, H.-T.; Nguyen, T.-K.; Inam, F.; Lee, J. A quasi-3D theory for vibration and buckling of functionally graded sandwich beams. *Compos. Struct.* **2015**, *119*, 1–12. [CrossRef]
34. Sobhy, M.; Radwan, A.F. A new quasi 3D nonlocal plate theory for vibration and buckling of FGM nanoplates. *Int. J. Appl. Mech.* **2017**, *9*, 1750008. [CrossRef]
35. Shahsavari, D.; Karami, B.; Fahham, H.R.; Li, L. On the shear buckling of porous nanoplates using a new size-dependent quasi-3D shear deformation theory. *Acta Mech.* **2018**, *229*, 4549–4573. [CrossRef]
36. Van Do, V.N.; Lee, C.-H. Quasi-3D higher-order shear deformation theory for thermal buckling analysis of FGM plates based on a meshless method. *Aerosp. Sci. Technol.* **2018**, *82*, 450–465.
37. Mashat, D.S.; Zenkour, A.M.; Radwan, A.F. A quasi 3-D higher-order plate theory for bending of FG plates resting on elastic foundations under hygro-thermo-mechanical loads with porosity. *Eur. J. Mech.-A/Solids* **2020**, *82*, 103985. [CrossRef]
38. Zenkour, A. Quasi-3D Refined Theory for Functionally Graded Porous Plates: Displacements and Stresses. *Phys. Mesomech.* **2020**, *23*, 39–53. [CrossRef]
39. Doan, T.N.; Thanh, N.T.; Van Chuong, P.; Tho, N.C.; Ta, N.T.; Nguyen, H.N. Analysis of stress concentration phenomenon of cylinder laminated shells using higher-order shear deformation Quasi-3D theory. *Compos. Struct.* **2020**, *232*, 111526. [CrossRef]
40. Akavci, S.; Tanrikulu, A. Static and free vibration analysis of functionally graded plates based on a new quasi-3D and 2D shear deformation theories. *Compos. Part B Eng.* **2015**, *83*, 203–215. [CrossRef]
41. Thai, H.-T.; Kim, S.-E. A simple quasi-3D sinusoidal shear deformation theory for functionally graded plates. *Compos. Struct.* **2013**, *99*, 172–180. [CrossRef]
42. Thai, C.H.; Ferreira, A.; Tran, T.; Phung-Van, P. A size-dependent quasi-3D isogeometric model for functionally graded graphene platelet-reinforced composite microplates based on the modified couple stress theory. *Compos. Struct.* **2020**, *234*, 111695. [CrossRef]
43. Neves, A.; Ferreira, A.; Carrera, E.; Cinefra, M.; Roque, C.; Jorge, R.; Soares, C. A quasi-3D hyperbolic shear deformation theory for the static and free vibration analysis of functionally graded plates. *Compos. Struct.* **2012**, *94*, 1814–1825. [CrossRef]
44. Reddy, B.S.; Kumar, J.S.; Reddy, C.E.; Reddy, K. Buckling analysis of functionally graded material plates using higher order shear deformation theory. *J. Compos.* **2013**, *2013*. [CrossRef]

45. Thai, H.-T.; Choi, D.-H. An efficient and simple refined theory for buckling analysis of functionally graded plates. *Appl. Math. Model.* **2012**, *36*, 1008–1022. [CrossRef]
46. Thinh, T.I.; Tu, T.M.; Quoc, T.H.; Long, N.V. Vibration and buckling analysis of functionally graded plates using new eight-unknown higher order shear deformation theory. *Lat. Am. J. Solids Struct.* **2016**, *13*, 456–477. [CrossRef]
47. Zenkour, A. A comprehensive analysis of functionally graded sandwich plates: Part 1—Deflection and stresses. *Int. J. Solids Struct.* **2005**, *42*, 5224–5242. [CrossRef]
48. Sobhy, M. Buckling and free vibration of exponentially graded sandwich plates resting on elastic foundations under various boundary conditions. *Compos. Struct.* **2013**, *99*, 76–87. [CrossRef]